Collection-limited theory interprets the extraordinary response of single semiconductor organic solar cells

Biswajit Ray[a,1], Aditya G. Baradwaj[b], Mohammad Ryyan Khan[a], Bryan W. Boudouris[b], and Muhammad Ashraful Alam[a,1]

[a]School of Electrical and Computer Engineering, Purdue University, West Lafayette, IN 47907; and [b]School of Chemical Engineering, Purdue University, West Lafayette, IN 47907

Edited by Mark A. Ratner, Northwestern University, Evanston, IL, and approved July 21, 2015 (received for review April 6, 2015)

The bulk heterojunction (BHJ) organic photovoltaic (OPV) architecture has dominated the literature due to its ability to be implemented in devices with relatively high efficiency values. However, a simpler device architecture based on a single organic semiconductor (SS-OPV) offers several advantages: it obviates the need to control the highly system-dependent nanoscale BHJ morphology, and therefore, would allow the use of broader range of organic semiconductors. Unfortunately, the photocurrent in standard SS-OPV devices is typically very low, which generally is attributed to inefficient charge separation of the photogenerated excitons. Here we show that the short-circuit current density from SS-OPV devices can be enhanced significantly (∼100-fold) through the use of inverted device configurations, relative to a standard OPV device architecture. This result suggests that charge generation may not be the performance bottleneck in OPV device operation. Instead, poor charge collection, caused by defect-induced electric field screening, is most likely the primary performance bottleneck in regular-geometry SS-OPV cells. We justify this hypothesis by: (*i*) detailed numerical simulations, (*ii*) electrical characterization experiments of functional SS-OPV devices using multiple polymers as active layer materials, and (*iii*) impedance spectroscopy measurements. Furthermore, we show that the collection-limited photocurrent theory consistently interprets typical characteristics of regular SS-OPV devices. These insights should encourage the design and OPV implementation of high-purity, high-mobility polymers, and other soft materials that have shown promise in organic field-effect transistor applications, but have not performed well in BHJ OPV devices, wherein they adopt less-than-ideal nanostructures when blended with electron-accepting materials.

exciton | charge collection | organic photovoltaic | solar cell | organic defects

The photovoltaic properties of semiconducting polymers arranged in a simple metal–polymer–metal sandwich structure were first demonstrated in 1993 by several groups (1–3). The efficiency values of these early photovoltaic (PV) cells were minuscule mainly because of the poor short-circuit current densities (J_{sc} ∼10 μA cm^{-2}) under standard 1 sun illumination. By definition,

$$J_{sc} \approx J_{ph}(V=0) = \eta_{ex}\eta_C J_{max}, \quad [1]$$

where $J_{ph}(V)$ is the voltage-dependent photocurrent, η_{ex} is the exciton diffusion-dissociation (or free-charge generation) efficiency, η_C is the charge (free-carrier) collection efficiency, and J_{max} is the maximum current density obtained by integrating absorption spectra ($J_{max} \sim 10-20$ mA cm^{-2} for typical semi-conducting polymers). The difference between J_{sc} and J_{max} was attributed to an inefficient η_{ex} (<0.1%) arising from ultrashort exciton diffusion lengths (∼10–15 nm) in semiconducting polymers and was eventually interpreted by Onsager's theory of geminate pair recombination (4–6). This classical interpretation assumes, on the other hand, that $\eta_C \sim 100\%$.

To improve η_{ex}, Heeger and co-workers (7) and Holmes and co-workers (8) introduced the concept of bulk heterojunction (BHJ) devices in 1995. Here, the active layer consists of two organic semiconductors: an electron-donating, hole-conducting (p-type) semiconducting polymer blended with an electron-accepting, electron-conducting (n-type) organic semiconductor. It was suggested that the interpenetrating bicontinuous morphology creates a distributed p–n heterojunction throughout the absorbing semiconducting active layer. This heterojunction (HJ) between the electron-donating and electron-accepting materials is able to dissociate excitons before they recombine, and therefore one expects and observes a higher η_{ex} and an improved J_{sc}. Once the nanostructure of the donor–acceptor blend was optimized by controlling the casting solution, deposition protocols, and postprocessing conditions, the BHJ-OPV led to the highest-performing polymer-based OPV devices ever reported in the literature (9–13). In fact, a number of groups have achieved $J_{sc} \sim J_{max}$ (14), implying nearly perfect exciton dissociation ($\eta_{ex} \approx 1$) and charge collection ($\eta_C \approx 1$).

It has long been recognized, however, that despite a high J_{sc}, a number of critical (and possibly fundamental) limitations of the BHJ concept will prevent the approach from ever achieving efficiency and reliability comparable to highly efficient inorganic solar cells. First, the energy band discontinuity (ΔE_c) at the HJ directly translates to an irretrievable loss of the open-circuit voltage, V_{oc} (15, 16), because electrons and holes recombine at the donor–acceptor interface (i.e., the cross-gap at the HJ) at energies lower than the optical gap of donor or acceptor (17). Second, the efficiencies of BHJ solar cells appear to be highly sensitive to the processing conditions [e.g., solution composition (18) and postprocessing annealing conditions (19)] and failure

Significance

We demonstrate that, instead of the charge generation mechanism, charge collection can readily explain the bottleneck toward higher efficiency single organic semiconductor based OPVs (SS-OPVs). This change in archetype has the potential to transform the design rules for materials used in OPV devices and would inspire searches for a completely different set of polymers for OPV cells. Furthermore, we believe that our findings will broaden the understanding of the physics of charge transport and the impact of charged defect states in organic electronic devices. Hence, this work should have deep and immediate impact on the chemists, materials scientists, and device physicists in the field and would be of broad interest to the organic electronics community.

Author contributions: B.R., B.W.B., and M.A.A. designed research; B.R., A.G.B., and M.R.K. performed research; B.R. and M.R.K. contributed new reagents/analytic tools; B.R., M.R.K., B.W.B., and M.A.A. analyzed data; and B.R., A.G.B., M.R.K., B.W.B., and M.A.A. wrote the paper.

The authors declare no conflict of interest.

This article is a PNAS Direct Submission.

[1]To whom correspondence may be addressed. Email: biswajit.025@gmail.com or alam@purdue.edu.

This article contains supporting information online at www.pnas.org/lookup/suppl/doi:10.1073/pnas.1506699112/-/DCSupplemental.

to achieve optimum morphology is reflected in very poor device efficiency (20, 21). Finally, because the activation energy of phase segregation is relatively small, the nanostructure continues to evolve (degrade) under standard operating conditions (22), shortening the useful lifetime of OPV technologies.

These fundamental limitations of BHJ-OPV devices suggest that the original SS-OPV concept should be reconsidered; specifically, the physical origin of the poor J_{sc} should be explained in much fuller detail. In this effort, we show that the main reason for poor J_{ph} in SS-OPV devices is the poor charge collection property (η_C) of the organic film. We establish this hypothesis by demonstrating a 100-fold improvement in J_{sc} of SS-OPV devices made of the commonly used semiconducting polymers poly[2-methoxy-5-(2-ethylhexyloxy)-1,4-phenylenevinylene] (MEH-PPV), poly(3-hexylthiophene) (P3HT), and poly[5,5′-*bis*(3-dodecyl-2-thienyl)-2,2’-bithiophene] (PQT-12) with inverted electrode configurations. This dramatic improvement in J_{sc} cannot be interpreted by the classical view of poor field-dependent η_{ex} in polymers. Furthermore, we used impedance spectroscopy and detailed optoelectronic numerical simulations to develop an alternate collection-limited model of OPV. The model allows us to reinterpret the classical experiments and help resolve a number of anomalous SS-OPV experiments (e.g., efficiency gain at lower intensity, voltage dependence of the reverse J_{ph}). Importantly, the numerical model, based exclusively on free-carrier transport, explains how the optoelectronic interplay defines the unconventional features in the external quantum efficiency (EQE) spectrum; indeed, the match between theory and experiments is remarkable. Bias-dependent EQE measurements further confirm a high rate of charge generation. Therefore, the proposed theory encourages the development of organic semiconductors with improved charge collection properties for highly efficient SS-OPVs. Such device configurations will ensure next-generation OPVs free of variability and/or reliability concerns associated with BHJ structures.

Key Experiment

The inverted device configuration has been studied widely for BHJ-OPV devices (23–25); however, its impact on SS-OPV cells has not been explored in full. Here, we perform a side-by-side comparison of the photovoltaic response for single polymer-based OPV devices with both the typical and inverted configurations. The device structures and the corresponding J-V characteristics (1 sun illumination) are shown in Fig. 1. This result establishes that there is a significant (~200-fold) improvement in the photocurrent for the inverted device configuration relative to the standard OPV device configuration for an SS-OPV cell. The improvement is highly reproducible and has been observed routinely in the all of the devices fabricated.

Interpretation of the Key Experiment

We invoke the free-carrier–based collection theory to explain the origin of significant increase of J_{sc} in the inverted structure. Because the interchange of contacts affects charge collection efficiency, one must reexamine the presumption that $\eta_C \sim 100\%$ by examining the field distribution within the polymer ($\eta_{C,E}$) and the alignment of the absorption and the collection zones (η_G).

Defect-Induced Band Bending. The energy bands of an OPV are frequently drawn assuming the metal–insulator–metal (MIM) model, where the active layer is modeled as defect-free intrinsic semiconductor (dashed lines of Fig. 1*B*) (26). In practice, the impedance spectroscopy data (see Fig. S1) indicate the presence of high density of defect states acting as p-type dopants in the semiconductor (27–30). Under solar illumination, these defects are filled by photoinduced electrons, and they form a space-charge region (with corresponding nonlinear bending of the energy band diagram) near the organic low work function metal (27) (the solid lines of Fig. 1*B*). The defect-induced band diagram associated with

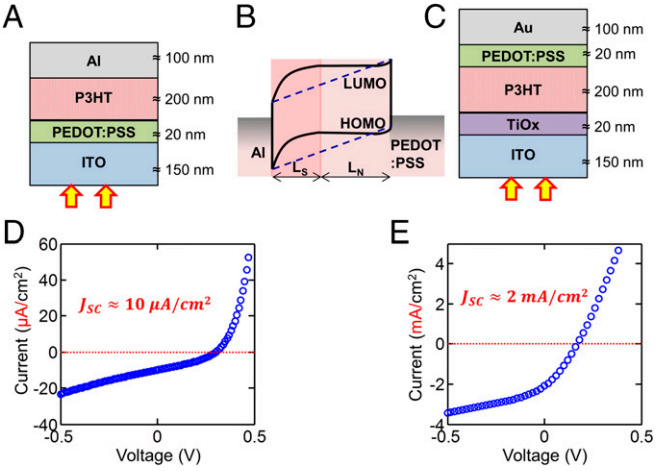

Fig. 1. (*A*) Device structure of the standard P3HT SS-OPV cell. (*B*) Energy band diagram of the absorbing layer, assuming MIM model (dashed line) vs. with band bending in the presence of charged defects (solid line). (*C*) Structure of the inverted SS-OPV with P3HT as the active material. (*D* and *E*) Corresponding J-V characteristics (under AM 1.5 illumination) of the standard and inverted devices, respectively.

direct and inverted structures is shown in Fig. 2. The field screening associated with the defects divides the active region into space-charge and field-free regions. This nonlinear band diagram implies $\eta_C < 1$, according to the following rationale.

Free-carrier transport in any semiconducting material can be described with the generalized drift-diffusion formalism. The electric field in the flat band region is negligible; therefore, charge transport in the field-free region is dictated exclusively by diffusion of the charges. The charge carrier mobility (or, alternatively, the charge carrier diffusion coefficient) in organic semiconductor is very low; therefore, the carrier diffusion length is small. This makes charge extraction from the neutral region highly inefficient. For example, the electron diffusion length in P3HT is estimated at $L_{diff} = \sqrt{D\tau_{rec}} = 5$ nm, for an electron mobility $\mu_e = 10^{-4}$ cm^2 V$^{-1}\cdot$s^{-1} and a typical recombination time $\tau_{rec} \sim 100$ ns. Due to such a low diffusion length, almost all of the photocarriers generated in the neutral region recombine before being collected by the electrodes. Conversely, charge collection in the space-charge region is enhanced greatly due to the presence of built-in electric field given by $E_{bi} \approx (V_{bi} - V)/L_S$, where V_{bi} is the built-in voltage and L_S is the length of the space-charge region. The electrostatic field drives the charge carriers by drift. This drift length is characterized by $L_{drift} = \mu E \tau_{rec}$, which typically is limited by the space-charge length. Thus, the collection length in typical polymer film is given by

$$L_C = \min\left(L_S, L_{drift}\right) + L_{diff} \le L_S + L_{diff}. \quad [2]$$

The corresponding defect-related collection efficiency, assuming uniform generation, is given by

$$\eta_{C,E} = \left(\frac{L_C}{L_{film}}\right) \le \left(\frac{L_S + L_{diff}}{L_{film}}\right). \quad [3]$$

In the *Supporting Information* (see Fig. S1), we show, by impedance spectroscopy measurements, that $L_S \le 30$ nm for a typical P3HT film and $L_{diff} \approx 5$ nm. Thus, Eq. **3** suggests that $\eta_{C,E} < 20\%$, for $L_{film} = 200$ nm in P3HT.

Nonuniform Exciton Generation. If the charge generation is spatially uniform, space-charge–limited collection itself does not explain the 100-fold difference in J_{sc} between the regular and the

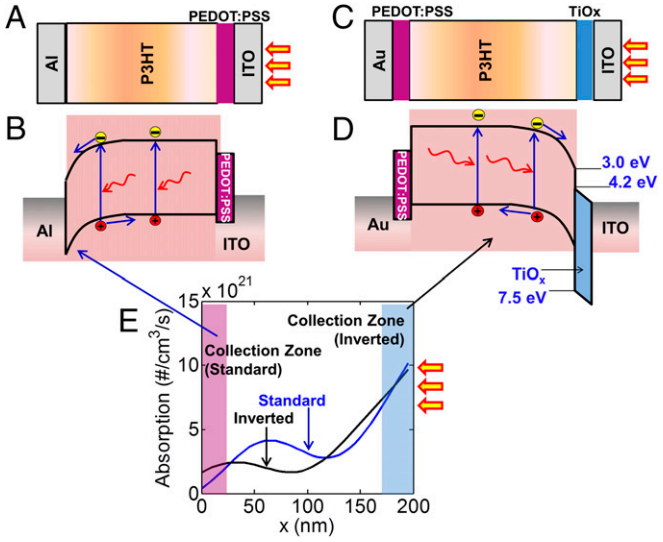

Fig. 2. (*A*) Device structure and (*B*) energy bands of SS-OPV devices are shown with the standard architecture electrode and (*C* and *D*) the inverted electrode configurations. Note that the space-charge layer, or band bending, is located at the back-contact side in standard electrode devices, but it is moved to the front-contact side in the inverted devices. A more detailed, numerically calculated band diagram is shown in Fig. S2*A*. (*E*) Light absorption profiles from the front (*Right*) to the back (*Left*) contact is shown for both the standard and inverted electrode devices. Even though absorption is comparatively smaller for the inverted device, its photocurrent is higher due to improved charge collection. The charge collection zones are indicated by shaded regions in the figure. Clearly, inverted devices collect more due to the higher absorption at the front side of the contact.

inverted structure. Indeed, η_{ex} and $\eta_{C,E}$ essentially are identical for both the structures because the intrinsic properties of the polymer do not depend on the position of the contacts. In addition, the V_{bi} for the two structures are comparable. The puzzle is resolved only when we use a standard numerical simulator to calculate the optical field profile inside the active region. Recall that semiconducting polymers generally are direct bandgap materials and, therefore, are strong absorbers of light. Most of the light is absorbed within the first few tens of nanometers of the film from the transparent contact of the cell. This is illustrated in Fig. 2*E*, where we plot the simulated absorption profile of P3HT photodiode for both standard and inverted electrode configurations (31).

With nonuniform generation, only those carriers generated within the space-charge region contribute to J_{ph}, and therefore Eq. **3** is rewritten as the following:

$$\eta_C \equiv \eta_{C,E}\eta_g = \left(\frac{L_C}{L_{film}}\right)\left(\frac{\overline{G}(x)}{\overline{G}(L_{film})}\right). \qquad [4]$$

Here, $\overline{G}(x)$ is the average generation in the film at a distance x from the contact that collects electrons.

In standard SS-OPV devices, the collection zone is located at the reflective-metal contact. This is because semiconducting polymers, being typically p-type, form the space-charge region at the contact with a work function nearer to vacuum (reflective-metal contact); unfortunately, the photogeneration at this back-contact is small. Thus, the collection efficiency given by Eq. **4** is very small, which explains the poor J_{ph} from an SS-OPV device using a regular architecture. Since all the OPV experiments in 1990s (1–3) utilized standard device configuration, the poor efficiency of SS-OPV is explained readily. In contrast, the peak of the spatial photogeneration and the charge-collection region are aligned for the inverted structure. The difference in η_C explains the difference in J_{sc}, implying high charge carrier generation for these polymers.

To confirm that the increase in J_{sc} in the inverted SS-OPV structure is not specific to P3HT, we fabricated and characterized a series of inverted cells using other well-known organic semiconductors, such as MEH-PPV and PQT-12. The results, summarized in Figs. S3–S6, show that the inverted configuration consistently produce high J_{sc} comparable to P3HT, and their J-V responses and the EQE results can be simply and self-consistently explained by the collection-limited theory described above.

Additional Explanation of Anomalous Results

High-Efficiency n-Type SS-OPV. For an n-type semiconductor [e.g., [6,6]-phenyl-C_{61}-butyric acid methyl ester (PCBM)], the space-charge region is formed at the hole collecting electrode (with a work function removed further from vacuum level), which is typically the transparent contact [i.e., indium-tin oxide (ITO), in most instances]. Thus, our theory predicts that the standard electrode configuration should lead to higher J_{ph} values in PCBM-only cells, and this prediction has recently been confirmed by several groups (32, 33). Interestingly, in PCBM-based SS-OPV devices (32, 33), the higher J_{ph} is explained by considering free-carrier generation with the assumption that in fullerene-only films exciton binding energy is small ($\eta_{ex} \approx 1$). Thus, our result on inverted P3HT-only devices confirms that free-carrier generation is significant even in the semiconducting polymer films and expands this paradigm of collection-limited theory of efficiency into a much broader regime.

Intensity-Dependent Efficiency Loss. A distinguishing feature for OPV technologies is that their power conversion efficiencies improve at lower illumination intensity. Our proposed collection-limited theory of photocurrent offers a consistent explanation for this trend. In Fig. 3, we plot the normalized solar cell performance metrics as a function of illumination intensity. Current density values are normalized by the corresponding light intensity values.

Ideally, J_{sc} (normalized) and the fill factor (FF) should remain constant with intensity, because generation is proportional to light intensity. The open-circuit voltage (V_{oc}) should increase slightly with intensity as the splitting of quasi-Fermi levels

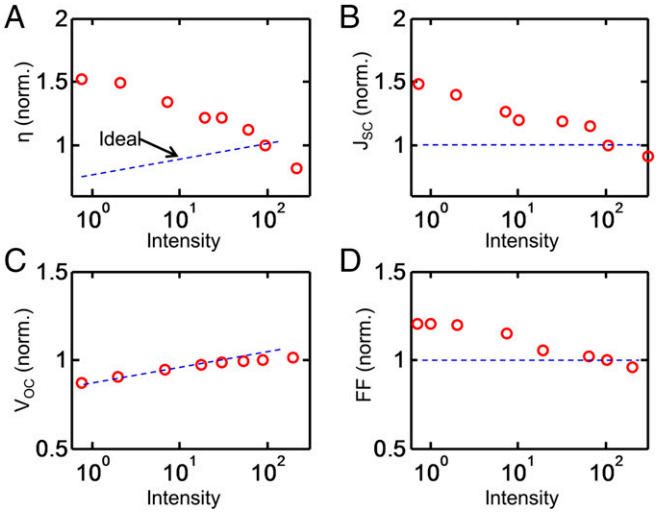

Fig. 3. Illumination intensity-dependent performance of organic solar cells. (*A*) Efficiency, (*B*) short-circuit current, (*C*) open-circuit voltage, and (*D*) FF as a function of illumination intensity. All of the performance metrics are normalized by performance values at intensity = 100 W cm^{-2}. Symbols are experimental results obtained from ref. 29 for OPV devices and lines correspond to results from the self-consistent numerical simulations for typical inorganic solar cells.

increases with light intensity. Thus, the overall efficiency should increase with intensity, as typically observed in all types of inorganic solar cells. However, as shown in Fig. 3, the J_{sc} (normalized) and FF of OPV cells decrease sharply with illumination intensity, which in turn reduces the efficiency.

These trends are consistent with the intensity-dependent charge collection efficiency model. In fact, by measuring the intensity-dependent capacitance–voltage (C-V) characteristics, one can determine the modulation of space-charge density and the corresponding change in collection lengths as a function of illumination intensity. In Fig. 4, we plot the measured C-V data as a function of illumination intensity for the same P3HT-based photodiode. From the slope of the Mott–Schottky plot (27), we find that the space-charge density increases with higher illumination intensity. This increase in space charge with illumination suggests that light illumination fills the deep level traps present in the polymeric semiconductor, and thereby increases the space-charge density (the full suite of impedance spectroscopy measurements is shown in the *Supporting Information*). Higher space-charge density screens the electric field within smaller length (L_S), thereby reducing the collection efficiency (see Eq. **3**, $\eta_C \propto L_S/L_{film}$).

Voltage-Dependent Reverse Photocurrent. Unlike BHJ-OPV cells, the J_{ph} of SS-OPV devices show a very strong voltage dependence, especially in the reverse bias regime (Fig. 5). It is argued that if the primary photoexcitation were free carriers, and if G is assumed uniform throughout the absorber layer, $J_{ph}(\propto qGL)$ should be field independent for negative voltages (5, 6, 34). Thus, a field-dependent J_{ph} is often referred to as an unambiguous signature for the exciton model, and generally explained by the voltage-dependent charge generation (or exciton dissociation) efficiency (η_{ex}) (5, 6, 34).

In Fig. 5, we provide a simpler explanation for the increase of J_{ph} in reverse bias, based on voltage-dependent collection efficiency (η_C), and without invoking any rate-limiting role of excitons. Fig. 5*A* shows the J-V characteristics for an inverted P3HT-based photodiode for negative applied voltages. Clearly, the magnitude of the current density increases greatly in the negative voltages. Three representative points in the J-V plot are taken to explain such voltage dependence. Fig. 5*C* shows the active layer band diagram for these three different negative voltages obtained by numerical simulation. The plot illustrates the fact that the space-charge length increases under reverse bias. Because the charge collection length is limited by the space-charge length, $L_C \approx L_S$, according to Eq. **3**, the collection efficiency, $\eta_C \propto L_C/L_{film}$, increases with negative voltages, explaining the increase in J_{ph}. The voltage-dependent modulation of L_S is confirmed by the C-V measurement on the photodiode (Fig. 5*B*). The close agreement between the theory and experiment in Fig. 5 supports our assertion that the voltage-dependent charge collection can consistently

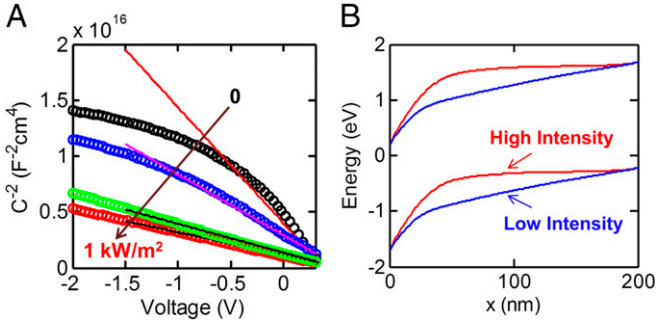

Fig. 4. (*A*) Measured C-V data of the P3HT photodiode with an increasing intensity of incoming radiation. (*B*) Corresponding energy band diagram of the active layer of the device at low and high light intensities, as calculated using a self-consistent simulation model.

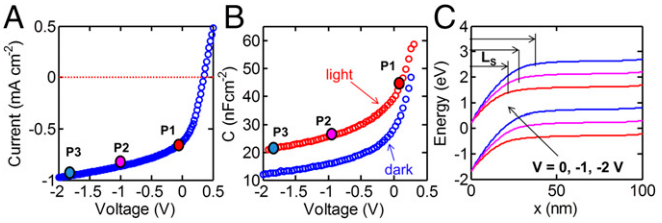

Fig. 5. Origin of voltage-dependent photocurrent. (*A*) Measured light J-V characteristics for an inverted P3HT SS-OPV diode. P1, P2, and P3 are three representative points on the J-V curve. (*B*) Measured C-V characteristics of the same diode. (*C*) Corresponding energy band diagrams of the active layer of the device at various reverse biases highlighting the difference in L_s for points P1, P2, and P3 in the J-V response curve.

interpret electrical performance of single-layer OPVs, and it does so without invoking any rate-limiting role of excitons.

Wavelength-Dependent Collection. We have conducted a rigorous optoelectronic numerical study of the inverted P3HT photodiode structure to elucidate the wavelength-dependent carrier collection. In fact, we can reproduce the experimental EQE spectral features based on our model, as shown in Fig. 6. Fig. 6*B* compares the normalized EQE response obtained from experiments (circles) and simulations (solid line). Next, we will use the proposed theory to explain the wavelength-dependent EQE shape at four representative wavelength positions marked as P1, P2, P3, and P4 in Fig. 6*B*. The related carrier generation profiles (i.e., the calculated photon absorption profiles) are shown in Fig. 6*C*, and the numerically found absorption spectrum for the various layers is shown in Fig. 6*A*.

For the case of point P4 ($\lambda = 350$ nm), there is very little absorption in P3HT (Fig. 6 *A* and *C*), as a large portion of the absorption occurs in ITO and TiO_x layers. Thus, the current, and hence the EQE, at this wavelength, is very low. Similarly for point P1, the low absorption near the band edge results in a low EQE.

The most interesting information, however, is obtained by comparing case P2 to case P3. The integrated absorption in the P3HT layers for case P3 ($\lambda \sim 500$ nm) and case P2 ($\lambda \sim 620$ nm) are comparable (Fig. 6*A*). The numerical simulation, however, suggests that whereas the integrated generation is similar, the spatial distributions are not. The photogeneration in the space-charge region for case P3 is higher compared with that of case P2, because a greater number of higher energy (i.e., shorter wavelength) photons are absorbed close to the interface inside the space-charge region. As a result, the collection-limited theory anticipates that the EQE for case P3 (shorter wavelength) would be significantly higher than that of case P2 (longer wavelength)—a prediction quantitatively validated by the measured EQE data shown in Fig. 6*B*. This result directly supports our collection-limited photocurrent model.

Discussion and Conclusions

We note that, in the inverted configuration, the TiO_x buffer layer creates an organic–inorganic hybrid bilayer. It may be argued reasonably that the efficiency gain in the inverted HJ arises from efficient dissociation of the photogenerated excitons by the TiO_x/polymer HJ. Here, we address this possibility with voltage-dependent EQE experiment and detailed numerical simulations to demonstrate that this is not necessarily the case. Fig. 7*A* shows EQE spectrum (at 0 V) (blue) and the EQE spectrum (at −1 V) (red) of the inverted P3HT-based SS-OPV device. The EQE(V = −1 V) is higher than the EQE(V = 0 V) for all wavelengths (i.e., carrier collection increases at all wavelengths for negative bias). However, the more informative value is the ratio of EQE(V = −1 V)/EQE(V = 0 V), as shown in Fig. 7*B*. Note

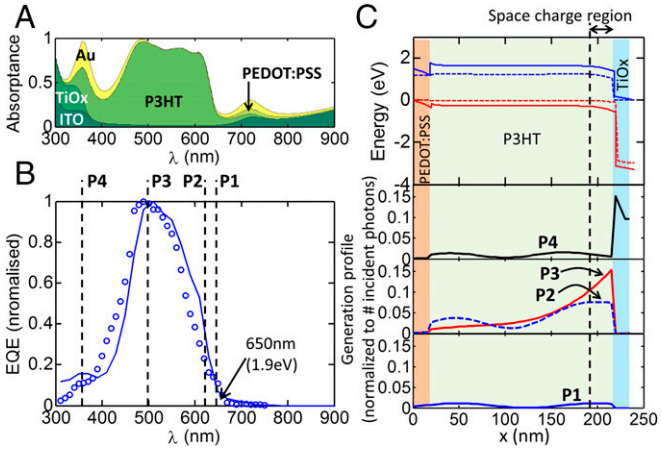

Fig. 6. (*A*) Numerically calculated absorption spectrum for the various layers of the OPV structure. (*B*) Normalized EQE response measured from the experimentally fabricated OPV devices (circles) is compared with the normalized numerically calculated EQE (solid line). (*C*) Band diagram under short-circuit condition is shown (*Top*). Also, photogeneration (normalized to the number of incident photons) profiles are shown at four different wavelengths as marked in *B*.

that by taking the ratio, we eliminate the parasitic absorption in the layers other than P3HT, and we remove also the variable absorption for different wavelengths. This allows us to focus exclusively on the carrier collection. According to generation-limited theory, the collection is expected to improve for higher energy incident photons ($\lambda < 550$ nm) as excitons at higher energies are more probable to be dissociated in the SS-OPV device. Remarkably, however, even at energies close to the band edge ~1.9 eV ($\lambda = 650$ nm), the EQE ratio is comparable to those at significantly higher energies. The uniform enhancement in EQE with negative bias, represented by the EQE(V = –1 V)/EQE(V = 0 V) ratio for a large range of wavelengths (up to the band edge), supports the possibility of high exciton dissociation rate even close to the bandgap.

Next, we provide three arguments supported by simulation results to further establish our hypothesis. First, we numerically simulate the photodiode response of Fig. 1 (Fig. S2) assuming only free-carrier transport without considering any role of TiO_x in exciton dissociation. The simple fact that the (exciton-free) free-carrier response properly captures the shape and the magnitude of the J-V characteristics seen in experiments (Fig. 1), immediately, yet indirectly, suggests that one need not invoke the exciton dissociation at TiO_x as a rate-limiting step. Second, the voltage-dependent modulation of electric field at the TiO_x–P3HT interface is negligible (as most of the voltage drops across the depletion region due to electric field screening by the space charge); therefore, the strong voltage dependence of the photocurrent cannot be interpreted by field-dependent exciton dissociation at the TiO_x–P3HT interface. Third, charge generation (or exciton dissociation) by the HJ should be proportional to the light intensity. However, Fig. 3 shows an efficiency loss at higher light intensity. Our collection-limited model consistently explains this observation.

The collection-limited theory of photocurrent discussed in this paper does not contradict the well-known notion of exciton formation in polymers, especially characterized under monochromatic low-level illumination. Under the broadband solar illumination, however, the excess energy of the photons incident upon the polymer may be sufficient to dissociate excitons (35–38). Moreover, impurities or dopants in the bulk of the polymer may provide another channel for efficient exciton dissociation into free carriers. Second, our EQE measurements indicate the transport gap and optical gap for the polymers considered differ by <0.1 eV, explaining facile dissociation of excitons into free carriers. This result is consistent with previous transient photoconductivity results from Heeger and co-workers (37, 39), but differs substantially from those obtained from photophysical experiments, such as ultraviolet photoelectron spectroscopy (UPS)/inverse photoemission spectroscopy (IPES) (40). Therefore, the relevance of these photophysical experiments in interpreting device performance needs to be reconciled in future work on this topic. Finally, it may be possible that the charge-generation-limited theory, appropriately and broadly modified, may eventually explain the results we have presented. We simply suggest that the expansive experimental and computational results presented in this paper are consistently and collectively explained by a simple charge-transport-limited theory.

Finally, based on the transport-limited theory of OPV devices, we suggest that the role of the HJ in BHJ devices is to minimize the free-carrier recombination by keeping the electrons and the holes isolated in their respective electron acceptor and electron donor channels. This type-II staggered band strategy removes minority carriers, and thereby improves the effective carrier diffusion in their respective channels regardless of the defect density within the active region. Therefore, materials with high absorption across a broad spectral range and with high-mobility, ambipolar behavior would be ideal for single-semiconductor inverted OPV devices. This critical change in paradigm could greatly alter the design strategy of macromolecular chemists.

In summary, we have shown that inefficient charge extraction is the origin of low J_{ph} in the standard SS-OPV device configuration. The charged defect states in the semiconductor screen the electric field within a few tens of nanometers of the electron-collecting contact, and thereby make charge extraction difficult. However, this extraction problem can be mitigated, in part, by the application of the correct electrode polarity relative to the incoming incident radiation for SS-OPV devices or by the insertion of closely spaced electrodes in the organic film (41). Therefore, our demonstration that charge extraction can be the key limiting step in these SS-OPV devices alters the molecular design considerations (e.g., highly crystalline, ambipolar polymers

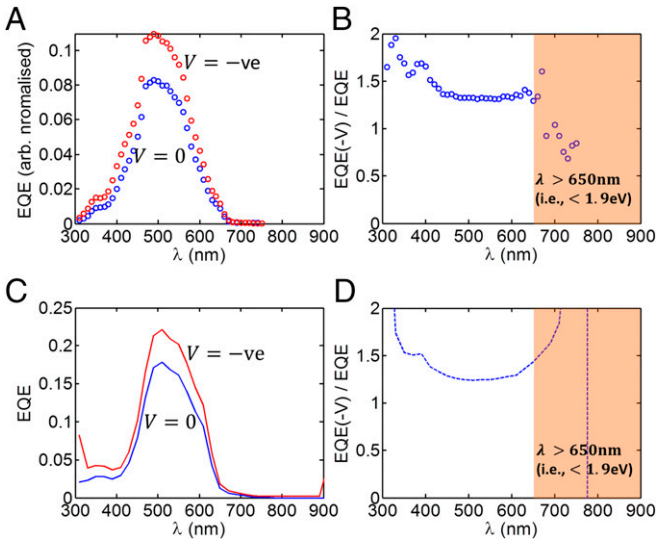

Fig. 7. (*A*) Measured EQE (blue) and reverse-bias EQE(–V) (red) responses are shown. (*B*) The ratio of EQE(V = –1 V)/EQE(V = 0 V) is shown. The ratio near the band edge (1.9 eV) represents bias-dependent carrier collection of photogenerated carriers near the band edge. The ratio is high, indicating good exciton dissociation at these energy levels as well. The EQE values for $\lambda > 650$ nm are very small and the ratio (in the shaded region) for this condition is not informative. (*C* and *D*) Corresponding simulated results. The trends from experiments are captured in our exciton agnostic, transport-limited model.

should be explored) of active layer polymers. In fact, these results suggest that several materials that are used in high-performance organic field-effect transistors could be implemented in OPV devices immediately as their miscibility and nanostructure with respect to an electron-accepting material (e.g., a fullerene derivative) are no longer of concern. In this way, the production of high-performance, reproducible, and long-lasting OPV devices could be on the near horizon.

ACKNOWLEDGMENTS. The work was supported by the Center for Re-Defining Photovoltaic Efficiency through Molecule Scale Control, an Energy Frontier Research Center funded by the US Department of Energy, Office of Science, and Office of Basic Energy Sciences under Award DE-SC0001085. The computational resources for this work were provided by the Network of Computational Nanotechnology under National Science Foundation Award EEC-0228390. A.G.B. and B.W.B. gratefully acknowledge the Air Force Office of Scientific Research Young Investigator Program (Grant FA9550-12-1-0243, Program Manager: Dr. Charles Lee) for support to perform device fabrication and characterization experiments.

1. Yu G, Zhang C, Heeger AJ (1994) Dual-function semiconducting polymer devices: Light-emitting and photodetecting diodes. *Appl Phys Lett* 64:1540–1542.
2. Antoniadis H, Hsieh BR, Abkowitz MA, Jenekhe SA, Stolka M (1994) Photovoltaic and photoconductive properties of aluminum/poly(p-phenylene vinylene) interfaces. *Synth Met* 62:265–271.
3. Marks RN, Halls JJM, Bradley DDC, Friend RH, Holmes AB (1994) The photovoltaic response in poly(p-phenylene vinylene) thin-film devices. *J Phys Condens Matter* 6:1379–1394.
4. Onsager L (1938) Initial recombination of ions. *Phys Rev* 54:554–557.
5. Barth S, Bässler H (1997) Intrinsic photoconduction in PPV-type conjugated polymers. *Phys Rev Lett* 79:4445–4448.
6. Däubler TK, Cimrová V, Pfeiffer S, Hörhold H-H, Neher D (1999) Electric field and wavelength dependence of charge carrier photogeneration in soluble poly(p-phenylenevinylene) derivatives. *Adv Mater* 11:1274–1277.
7. Yu G, Gao J, Hummelen JC, Wudl F, Heeger AJ (1995) Polymer photovoltaic cells: Enhanced efficiencies via a network of internal donor-acceptor heterojunctions. *Science* 270:1789–1791.
8. Halls J, et al. (1995) Efficient photodiodes from interpenetrating polymer networks. *Nature* 376(6540):498–500.
9. Shaheen SE, et al. (2001) 2.5% efficient organic plastic solar cells. *Appl Phys Lett* 78(6): 841–843.
10. Li G, et al. (2005) High-efficiency solution processable polymer photovoltaic cells by self-organization of polymer blends. *Nat Mater* 4(11):864–868.
11. Ma W, Yang C, Gong X, Lee K, Heeger AJ (2005) Thermally stable, efficient polymer solar cells with nanoscale control of the interpenetrating network morphology. *Adv Funct Mater* 15:1617–1622.
12. Peet J, et al. (2007) Efficiency enhancement in low-bandgap polymer solar cells by processing with alkane dithiols. *Nat Mater* 6(7):497–500.
13. Boudouris BW (2013) Engineering optoelectronically active macromolecules for polymer-based photovoltaic and thermoelectric devices. *Curr Opin Chem Eng* 2:294–301.
14. Park SH, et al. (2009) Bulk heterojunction solar cells with internal quantum efficiency approaching 100%. *Nat Photonics* 3(5):297–302.
15. Rand BP, Burk DP, Forrest SR (2007) Offset energies at organic semiconductor heterojunctions and their influence on the open-circuit voltage of thin-film solar cells. *Phys Rev B* 75:115327.
16. Koster LJA, Shaheen SE, Hummelen JC (2012) Pathways to a new efficiency regime for organic solar cells. *Adv Energy Mater* 2:1246–1253.
17. Ray B, Lundstrom MS, Alam MA (2012) Can morphology tailoring improve the open circuit voltage of organic solar cells? *Appl Phys Lett* 100(1):013307.
18. Mayer AC, et al. (2009) Bimolecular crystals of fullerenes in conjugated polymers and the implications of molecular mixing for solar cells. *Adv Funct Mater* 19(8):1173–1179.
19. Ray B, Nair PR, Alam MA (2011) Annealing dependent performance of organic bulk-heterojunction solar cells: A theoretical perspective. *Sol Energy Mater Sol Cells* 95: 3287–3294.
20. Renz JA, et al. (2009) Multiparametric optimization of polymer solar cells: A route to reproducible high efficiency. *Sol Energy Mater Sol Cells* 93(4):508–513.
21. Alstrup J, Jørgensen M, Medford AJ, Krebs FC (2010) Ultra fast and parsimonious materials screening for polymer solar cells using differentially pumped slot-die coating. *ACS Appl Mater Interfaces* 2(10):2819–2827.
22. Ray B, Alam MA (2011) A compact physical model for morphology induced intrinsic degradation of organic bulk heterojunction solar cell. *Appl Phys Lett* 99(3):033303.
23. White MS, Olson DC, Shaheen SE, Kopidakis N, Ginley DS (2006) Inverted bulk-heterojunction organic photovoltaic device using a solution-derived ZnO underlayer. *Appl Phys Lett* 89(14):143517.
24. Kim CS, Kim JB, Lee SS, Kim YS, Loo Y-L (2009) Sequence of annealing polymer photoactive layer influences the air stability of inverted solar cells. *Org Electron* 10:1483–1488.
25. He Z, et al. (2012) Enhanced power-conversion efficiency in polymer solar cells using an inverted device structure. *Nat Photonics*, 10.1038/nphoton.2012.190.
26. Koster LJA, Smits ECP, Mihailetchi VD, Blom PWM (2005) Device model for the operation of polymer/fullerene bulk heterojunction solar cells. *Phys Rev B* 72(8):085205.
27. Ray B, Baradwaj AG, Boudouris BW, Alam MA (2014) Defect characterization in organic semiconductors by forward bias capacitance–voltage (FB-CV) analysis. *J Phys Chem C* 118:17461–17466.
28. Carr JA, Chaudhary S (2013) On the identification of deeper defect levels in organic photovoltaic devices. *J Appl Phys* 114:064509.
29. Li JV, et al. (2011) Simultaneous measurement of carrier density and mobility of organic semiconductors using capacitance techniques. *Org Electron* 12:1879–1885.
30. Nikiforov MP, et al. (2013) Detection and role of trace impurities in high-performance organic solar cells. *Energy Environ Sci* 6:1513–1520.
31. Pettersson LAA, Roman LS Inganas O. (1999) Modeling photocurrent action spectra of photovoltaic devices based on organic thin films. *J Appl Phys* 86(1):487–496.
32. Yang B, et al. (2013) Solution-processed fullerene-based organic Schottky junction devices for large-open-circuit-voltage organic solar cells. *Adv Mater* 25(4):571.
33. Zhang M, Irfan, Ding H, Gao Y, Tang CW (2010) Organic Schottky barrier photovoltaic cells based on MoOx/C60. *Appl Phys Lett* 96(18):183301.
34. Hendry E, Schins JM, Candeias LP, Siebbeles LDA, Bonn M (2004) Efficiency of exciton and charge carrier photogeneration in a semiconducting polymer. *Phys Rev Lett* 92(19):196601.
35. Bakulin AA, et al. (2012) The role of driving energy and delocalized states for charge separation in organic semiconductors. *Science* 335(6074):1340–1344.
36. Coffey DC, et al. (2012) An optimal driving force for converting excitons into free carriers in excitonic solar cells. *J Phys Chem C* 116:8916–8923.
37. Gong X, et al. (2011) Bulk heterojunction solar cells with large open-circuit voltage: Electron transfer with small donor-acceptor energy offset. *Adv Mater* 23(20):2272–2277.
38. Chan W-L, Ligges M, Zhu X-Y (2012) The energy barrier in singlet fission can be overcome through coherent coupling and entropic gain. *Nat Chem* 4(10):840–845.
39. Lee CH, Yu G, Moses D, Heeger AJ (1994) Picosecond transient photoconductivity in poly(p-phenylenevinylene). *Phys Rev B Condens Matter* 49(4):2396–2407.
40. Guan Z-L, et al. (2010) Direct determination of the electronic structure of the poly(3-hexylthiophene):phenyl-[6,6]-C61 butyric acid methyl ester blend. *Org Electron* 11:1779–1785.
41. Ray B, Khan MR, Black C, Alam MA (2013) Nanostructured electrodes for organic solar cells: Analysis and design fundamentals. *IEEE J Photovolt* 3:318–329.
42. Gregg BA (2009) Charged defects in soft semiconductors and their influence on organic photovoltaics. *Soft Matter* 5:2985–2989.
43. Nalwa KS, Mahadevapuram RC, Chaudhary S (2011) Growth rate dependent trap density in polythiophene-fullerene solar cells and its implications. *Appl Phys Lett* 98(9):093306.
44. Boix PP, et al. (2009) Determination of gap defect states in organic bulk heterojunction solar cells from capacitance measurements. *Appl Phys Lett* 95(23):233302.
45. Nicolai HT, et al. (2012) Unification of trap-limited electron transport in semiconducting polymers. *Nat Mater* 11(10):882–887.
46. Kirchartz T, et al. (2012) Sensitivity of the Mott–Schottky analysis in organic solar cells. *J Phys Chem C* 116(14):7672–7680.
47. Sze SM (1981) *Physics of Semiconductor Devices* (John Wiley & Sons, New York).
48. Unalan HE, et al. (2008) Flexible organic photovoltaics from zinc oxide nanowires grown on transparent and conducting single walled carbon nanotube thin films. *J Mater Chem* 18(48):5909–5912.
49. Ray B, Alam MA (2013) Achieving fill factor above 80% in organic solar cells by charged interface. *IEEE J Photovolt* 3:310–317.
50. Ray B, Alam MA (2012) Random vs regularized OPV: Limits of performance gain of organic bulk heterojunction solar cells by morphology engineering. *Sol Energy Mater Sol Cells* 99:204–212.